

Large magnetoresistance in carbon-coated Ni/NiO nanoparticles

SUBIR ROY, RAJESH KATOCH and S ANGAPPANE*

Centre for Nano and Soft Matter Sciences (CeNS), Jalahalli, Bangalore 560013, India

*Author for correspondence (angappane@cens.res.in)

MS received 11 May 2018; accepted 16 July 2018; published online 8 September 2018

Abstract. We report here a large magnetoresistance (MR) observed in carbon-coated Ni/NiO nanostructures synthesized by a chemical method. The crystalline nature and particle size of the graphitic-carbon-coated Ni/NiO nanostructure was investigated by X-ray diffraction study and field emission scanning electron microscope images. The Raman spectroscopy confirms the presence of graphite layer over the Ni/NiO nanostructure. The field-cooled (FC) magnetic hysteresis curves show exchange bias effect suggesting possible Ni/NiO core-shell structure. The temperature-dependent magnetization data show bifurcation in FC-zero-field-cooled curves, indicating the superparamagnetic behaviour and competing ferromagnetic (FM) and antiferromagnetic interactions in the nanocomposite. MR studies show a large negative MR of $\sim 20\%$ at 18 K and $\sim 4.2\%$ at room temperature, revealing significant enhancement of FM interactions at low temperatures and spin-dependent tunnelling of current through the nanocomposite.

Keywords. Magnetoresistance; exchange bias; nanoparticles.

1. Introduction

The magnetic-field-induced change in resistance, i.e., magnetoresistance (MR), is extremely important for high-density data storage, spin valve devices and various sensing applications [1–3]. When the MR becomes very large, it is called as giant magnetoresistance (GMR), which has tremendous demand for the development of high-density data storage in computer hard drive and other spintronic devices [4]. The GMR is also getting intense attention in bio-molecular sensing because of its utility in making easy-to-use, point-of-care and hand-held devices [5]. A large change in resistance was observed in Fe/Cr superlattices with the application of external magnetic field, which was considered as the GMR for the first time [6]. The MR can originate due to multiple reasons, such as bending of carrier trajectories [7], narrowing of hopping paths due to Zeeman splitting [8] and localized wavefunction shrinkage [9]. For a magnetic multilayer system, the parallel alignment of ferromagnetic (FM) moments in magnetic field reduces the spin-electron scattering, resulting in decrease of resistance of the system, which leads to negative MR [10]. Besides the multilayers, the MR and GMR were observed also in a nano-granular system [11]. The electrical resistance changes due to the spin-dependent scattering of electrons by the FM moments [12]. The factor that is crucial for the spin-dependent scattering is $\langle \cos \phi_{ij} \rangle$, where ϕ_{ij} represents the angle between the magnetization axes of two nanoparticles (NPs) [11]. In magnetite NPs, the spin-polarized electron transport through the grains of the particles was attributed to the origin of negative MR [13]. The FM NPs

embedded in conducting matrix mostly show large value of MR [14], while the FM NPs embedded in non-conducting matrix show tunnel magnetoresistance (TMR) [15]. In TMR, the electron tunnelling takes place through a thin insulating layer placed between two FM layers. The tunnelling of electron depends on the relative alignment of the FM moments [16]. The tunnelling current is higher for parallel alignment of FM moments and is lower for antiparallel alignments. The TMR observed in magnetic NPs is of great interest because of its surface-dependent properties [17]. In magnetic NPs the inter-particle interactions play a crucial role in magnetic as well as magneto-electrical properties [18]. Hence, the different types of MR observed in magnetic NPs are of great interest from experimental as well as theoretical aspects.

In this paper, we report MR study of carbon-coated Ni/NiO NPs. A large negative MR was observed in our sample, which is attributed to the electron-spin scattering and spin-dependent tunnelling of current through the NPs.

2. Experimental

The carbon-coated Ni/NiO (C-Ni/NiO) nanocomposite was synthesized using nickel(II) nitrate hexahydrate (Sigma-Aldrich, 99.99%), polyvinyl alcohol (PVA, Sigma-Aldrich, 99% hydrolysed), and graphite powder (Alfa Aesar, 99%); 0.25 M solution of $\text{Ni}(\text{NO}_3)_2 \cdot 6\text{H}_2\text{O}$ was prepared by dissolving 0.727 g of $\text{Ni}(\text{NO}_3)_2 \cdot 6\text{H}_2\text{O}$ in 10 ml of millipore water under stirring at 50°C for 1 h. Separately, 0.5 g of PVA and 0.06 g of graphite were mixed in 20 ml of millipore water

under stirring at 70°C for 3 h. Then, the nickel nitrate solution and the PVA-graphite solution were mixed by magnetic stirring for 3 h at 70°C to get a homogeneous mixture. After that, the temperature of the mixture was increased to 150°C to evaporate the solvent. The solid complex was collected and dried by keeping the sample in a hot air oven at 100°C for 1 h. Finally, the solid complex was annealed at 400°C in air for 2 h at the heating rate of 3°C min⁻¹ to get the powder sample of carbon-coated Ni/NiO nanocomposite.

The crystal structure of the nanocomposite was characterized using a Rigaku SmartLab X-ray diffractometer and Cu K α radiation. The particle size and surface morphology were studied using a MIRA3 LMU (TESCAN) field emission scanning electron microscope (FESEM). Raman spectroscopy study was carried out using a Horiba XploRE Plus Raman instrument with a 532 nm laser source. The magnetic properties were investigated using a Quantum Design MPMS-XL SQUID magnetometer. The zero field cooled (ZFC) and field-cooled (FC) magnetization measurements were carried out by cooling the sample from 380 to 10 K without and with a cooling magnetic field, respectively. To measure the MR, a pellet was prepared by cold pressing using a hydraulic press followed by annealing at 450°C for 2 h in air for better grain connectivity. A Keithley 6221 current source, Keithley 2182A nanovoltmeter and an electromagnet (Model HEM 150; Polytropic Corporation, India) with bipolar power supply were used for MR study. The low-temperature MR was measured using a closed-cycle refrigerator (Janis Research Company, USA).

3. Results and discussion

3.1 Structural characterization

The X-ray diffraction pattern of the C-Ni/NiO nanocomposite in figure 1 clearly shows the peaks corresponding to graphite, Ni and NiO. The diffraction peak at $2\theta \sim 26.41^\circ$ corresponds to the (002) plane and hexagonal phase of graphite with $P6_3/mmc$ space group (JCPDS no. 041-1487). The diffraction peaks of NiO corresponding to the reflections from (111), (200), (220), (311) and (222) crystallographic planes indicate the cubic structure with $Fm\bar{3}m$ space group symmetry (JCPDS no. 047-1049). Also, the formation of cubic Ni crystals is clear from the diffraction peaks at 44.46°, 51.74° and 76.3° corresponding to the (111), (200) and (220) crystalline planes, respectively (JCPDS no. 004-0850). The crystallite sizes of Ni and NiO were calculated using the Scherrer equation [19]

$$d = \frac{K\lambda}{\beta \cos \theta}, \quad (1)$$

where 'd' represents the average crystallite size, 'K' is the Scherrer constant, ' λ ' the wavelength of Cu K α radiation and ' β ' the full-width at half-maximum (FWHM) of the diffraction peaks. The calculated crystallite sizes of Ni and NiO

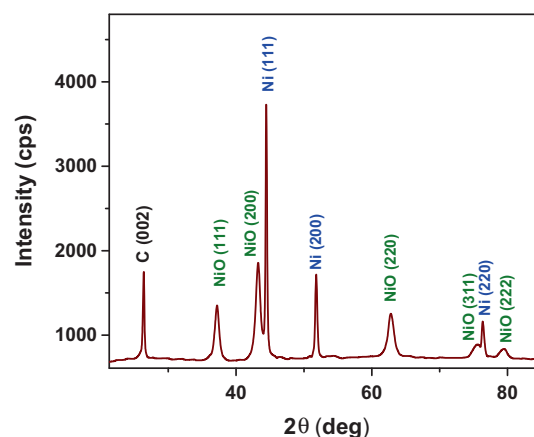


Figure 1. X-ray diffraction data of C-Ni/NiO nanocomposite.

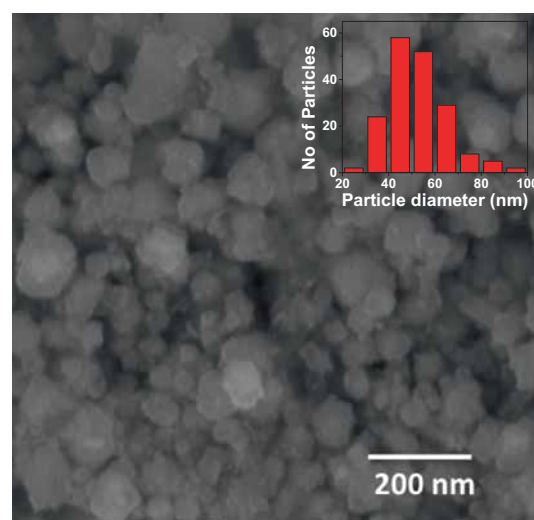


Figure 2. FESEM image of the C-Ni/NiO nanocomposite. Inset shows the particle size distribution.

were found to be 43 and 14 nm, respectively. Figure 2 shows the FESEM image of the nanocomposite. It is clear from the micrograph that the particles are nearly spherical in shape and the average particle size is about 50 nm.

3.2 Raman spectroscopy

The room-temperature Raman spectra of the carbon-coated Ni/NiO nanocomposite are shown in figure 3. There are several peaks in the Raman spectra arising from the various vibrational states of NiO nanocrystals and graphite layers. The first five peaks, i.e., one photon (1P) transverse optical (TO) mode at 384 cm⁻¹, 1P longitudinal optical (LO) mode at 521 cm⁻¹, 2P (TO) mode at 689 cm⁻¹, 2P TO + LO at 853 cm⁻¹ and 2P LO mode at 1069 cm⁻¹, are due to the presence of NiO. The broad nature of the 1P and 2P vibrational peaks and the absence of two magnon (2M) modes

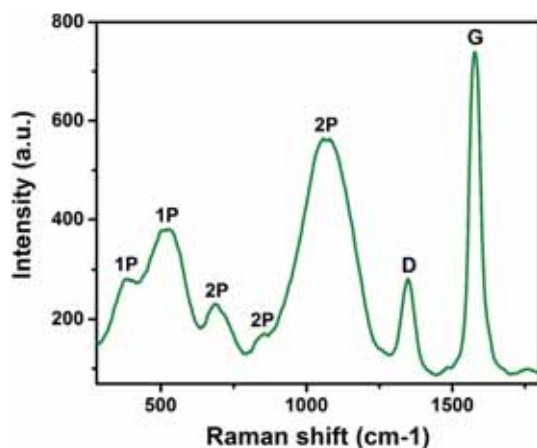


Figure 3. Room-temperature Raman spectra of C-Ni/NiO nanocomposite.

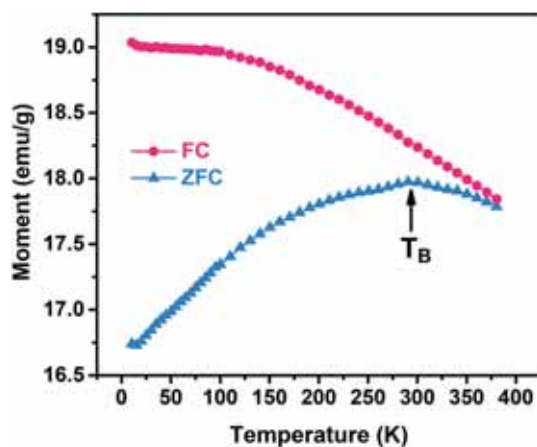


Figure 4. ZFC and FC magnetization curves of C-Ni/NiO nanocomposite.

are a signature of the formation of NiO nanocrystals [20]. The Raman peak at $\sim 1580\text{ cm}^{-1}$ represents the first allowed band or G band of graphite, which comes from the stretching of sp^2 bonds of the carbon atoms. The presence of D band (defect band) nearly at 1350 cm^{-1} signifies the disordered local arrangement of atoms in graphite, which could be due to the formation of nanographite [21].

3.3 Magnetic characterization

Figure 4 shows the temperature-dependent magnetization curve under ZFC and FC conditions with the applied field of $\sim 500\text{ Oe}$. The FC magnetization increases monotonically with the reduction of temperature from 380 to 100 K; after this, it gets almost saturated up to 20 K. With the decrease of temperature under FC condition, the disorder in the magnetic moments of the particles starts reducing gradually and the moments achieve an aligned state at low temperature [22].

In the ZFC curve, during cooling, the magnetization increases and reaches a maximum value at $\sim 290\text{ K}$, which represents the blocking temperature (T_B) of the sample. Below T_B , the sample is in a blocked state, due to freezing of moments. Above T_B , the NPs show superparamagnetic (SPM) behaviour and the magnetic moment decreases due to thermal fluctuations [23]. SPM is one of the commonly observed behaviour in magnetic NPs, where the particle size becomes comparable to the domain size of that material [23]. It was observed that the SPM nature and blocking temperature change with the change of particle sizes [24]. The Ni NP of average radius $\sim 3\text{ nm}$ embedded in SiO_2 showed SPM behaviour with blocking temperature of $\sim 20\text{ K}$ [25]. The SPM nature in Ni NP was observed also for the particles of size $\sim 4.2\text{ nm}$ at 32 K [26]. There are further reports on systems where the SPM behaviour of Ni NP is found in very smaller size ($\sim 4\text{ nm}$) particles with blocking temperature also at very low value ($\sim 4.5\text{ K}$) [27]. For NiO NPs, Duan *et al* [28] report that the T_B increases from 19.8 to 161 K with the increase of particle size from 3.5 to 12.4 nm. It was also observed that the value of T_B changes due to the inter-particle interactions among the NiO NPs [29]. In the Ni/NiO nanocomposite, the average SPM blocking temperature was attributed to the major contribution from the NiO component [30]. All these observations illustrate the possible reasons behind the broad peak in ZFC curve at comparatively higher temperature in our C-Ni/NiO nanocomposite. Hence, the T_B observed in our sample near room temperature reflects the contribution of NiO component in the nanocomposite. At temperatures higher than T_B , thermal energy increases the random fluctuations of the moments, and results in the decrease of magnetization slowly at higher temperature [31]. With the decrease of temperature below T_B , the magnetization was found to decrease monotonically. In case of antiferromagnetic (AFM) materials, the magnetization was found to decrease linearly with the decrease of temperature [32]. The decreasing nature of the magnetization with the decrease of temperature was attributed to the freezing of uncompensated moments [32].

The room-temperature (300 K) and low-temperature (10 K) magnetic hysteresis curves ($M-H$) of carbon-coated Ni/NiO are shown in figure 5. The $M-H$ curve shows sharp increase of moments with the increase of field and almost saturates at a moderate field ($>3.5\text{ kOe}$). The saturation magnetization value indicates that the large contributions to the magnetic moments come from Ni content of the sample. A similar kind of FM nature in Ni/NiO nanocomposite was reported by several groups [22,33–35]. Generally, bulk Ni shows saturation magnetization of $\sim 55\text{ emu g}^{-1}$ [36], but in our sample the presence of other components (NiO and graphite layer) results in the significant reduction of moment. Also, the large surface area of the NPs generates a large number of disordered surface spins, which reduces the net magnetic moment [37]. The magnetic moment and coercivity are found to be higher at low-temperature (10 K) than room-temperature (300 K) measurement, which could be due to the reduction in thermal fluctuation of spins and defect density.

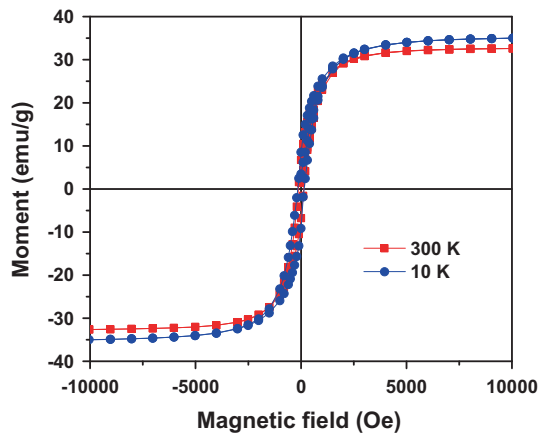


Figure 5. $M-H$ loop of C-Ni/NiO nanocomposite at 300 and 10 K.

Ideally, for monodisperse and non-interacting identical particles with zero anisotropy, the coercivity will be zero above blocking temperature and non-zero below it. In SPM materials, coercivity magnitude depends on the frequency of applied field, particle size and morphology, etc. In this work, the nanocomposite consists of NPs, which, although individually are of a single domain, show appreciable size and shape distribution. This explains the observation of significant coercivity even beyond the blocking temperature (300 K). Figure 6 shows the FC $M-H$ curve of the sample, where the sample was cooled from 300 to 10 K in the applied field of 1 T. In FM-AFM structures, cooling under a field results in exchange bias (EB) effect, which causes the $M-H$ loop to shift towards one direction of the field axis. To calculate the amount of loop shift (H_E), we used the equation,

$$H_E = \frac{(H_{C1} - H_{C2})}{2}, \quad (2)$$

where H_{C1} and H_{C2} are the intersecting points of $M-H$ curve to the field axis. Using the values of H_{C1} (200 Oe) and H_{C2} (−352 Oe), we find that the hysteresis loop shifts by 76 Oe along the field axis. The EB effect is explained by the exchange interaction between the FM and AFM interfaces, where the pinning of soft FM spins by the hard AFM spins during cooling results in the loop shift of $M-H$ curve [38]. The EB effect was first reported by Meiklejohn and Bean, where Co NPs were partially oxidized to form CoO at the surface to form a core-shell structure of Co/CoO. They explained the loop shift in the core-shell NP system by exchange interaction between the FM core and AFM shell [39]. Del Bianco *et al* [40] reported EB effect in Ni/NiO core-shell NPs, where the milled NiO powder was partially reduced by H_2 atmosphere to form the core-shell structure. For Ni/NiO NPs, Sharma *et al* [41] reported that the EB effect varies with the concentration of Ni in the sample. They observed maximum EB field (~ 2.2 kOe) for less Ni concentration (almost 0%) and the

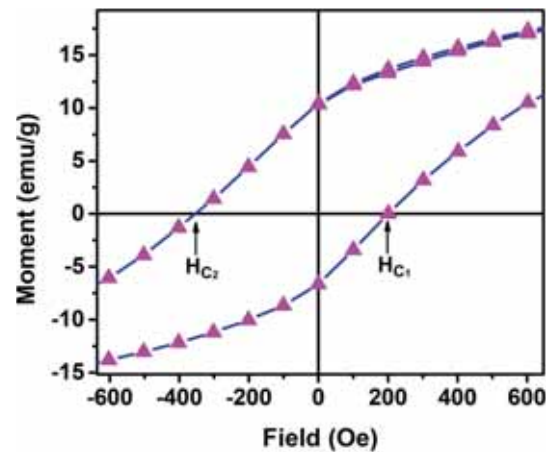


Figure 6. Exchange bias effect of C-Ni/NiO nanocomposite in a cooling field of 1 T.

EB field was minimum (~ 0.07 kOe) for the Ni concentration of 32%. Notably, the EB field of nearly 70 Oe observed in Ni/NiO NPs having 32% Ni concentration is comparable to the EB effect observed in our study on carbon-coated Ni/NiO NPs. The very small EB effect observed in core-shell Ni/NiO NPs synthesized by a microwave-assisted chemical route was attributed to the amorphous nature of NiO shell [33]. Del Bianco *et al* also reported that for Ni/NiO core-shell nanostructure, the lattice mismatch and topological disorder at the interface was responsible for the absence of EB effect above 200 K. This implies that one of the most important factors affecting the EB effect in Ni/NiO NPs is the roughness of the FM-AFM interface, which is controlled by the overall crystallinity of the core and shell. In this study, Ni and NiO phases were found to be crystalline as revealed in XRD and Raman measurements. Also, we found that average grain size was around 50 nm, for which the NiO remains AFM below T_B [42]. Below T_B , the NiO moments are blocked and fluctuations cease, giving rise to finite exchange bias by pinning the FM Ni moments. For $T_B < T < T_N$, AFM NiO moments are subject to SPM fluctuations and exchange bias vanishes. Thus, the EB effect observed in our sample possibly arises due to the core-shell structure of Ni/NiO with good crystalline nature and lattice plane matching of Ni and NiO layers.

3.4 MR characterization

Figure 7 shows the MR of carbon-coated Ni/NiO NPs at room temperature (300 K) and at low temperature (18 K). MR is defined as the percentage change of resistance of the sample in external magnetic field,

$$MR(\%) = \frac{R(H) - R(0)}{R(0)} \times 100, \quad (3)$$

where $R(H)$ and $R(0)$ are the resistance of the sample in field H and zero magnetic field, respectively. In our sample,

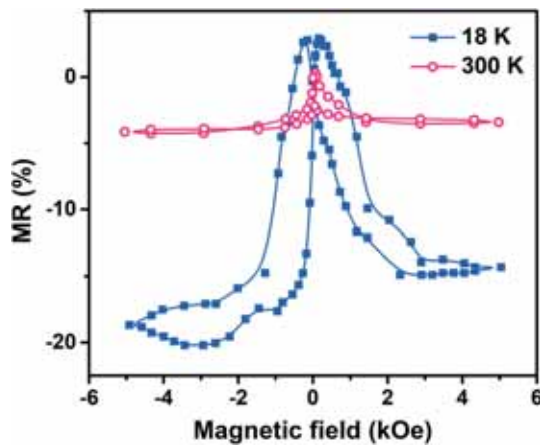


Figure 7. MR of C-Ni/NiO nanocompacts at 300 and 18 K.

the room-temperature (300 K) measurement shows $\sim 4.2\%$ decrease of resistance (negative MR) in 5 kOe external magnetic field, whereas the MR increases to $\sim 20.4\%$ at 18 K. To the best of our knowledge, such large negative MR ($\sim 20.4\%$) in graphitic-carbon-coated Ni/NiO nanocomposite at low temperature (18 K) has not been reported earlier. Parkin *et al* [43] reported GMR effect in FM–AFM multilayer system at room temperature, as well as at low temperature (4.2 K). They showed 65% saturation MR at 295 K, whereas the saturation MR increased to 115% at 4.2 K. In magnetic multilayers, the origin of GMR was explained on the basis of the relative orientation of the electron spin and the direction of magnetization of the multilayer. The effect is stronger when the electron spin and the magnetization direction of the layer are parallel and weaker for antiparallel alignment [44]. Additionally, GMR can also be the result of increased interfacial roughness for multilayer systems [45]. GMR effect is observed also in magnetic granular systems, where it originates due to scattering from nonaligned magnetic particles [11]. For instance, in epitaxial Co/Cu and Co/Ag granular alloys the GMR of ~ 50 and $\sim 70\%$ were observed, respectively, at 4.2 K. Likewise, in NPs, Liu *et al* [12] reported that the magnetite (Fe_3O_4) NP of size 8–9 nm shows MR as well as SPM property above 200 K. They found MR of 4.5% at 300 K and it was increased to 8.6% at 200 K. An MR of 10% was observed in fullerene-like carbon (graphite)-coated core-shell Ni NPs at 4 K, which was ascribed to the alignment of moments along the field direction [46]. For Ni/NiO nano-granular system, typically 0.2–0.5% negative MR was observed at 5 K [40]. However, the graphitic-carbon-coated Ni/NiO core-shell NPs were found to have large negative MR ($\sim 10\%$) even at room temperature [22]. The graphite coating over the Ni/NiO nanocomposite plays an important role in inter-bridging the grains and it also forms a tunnelling barrier between the grains. Under the influence of external magnetic field, spin-polarized Ni ($3d^9$) electrons tunnel across the barrier, resulting in enhanced MR response.

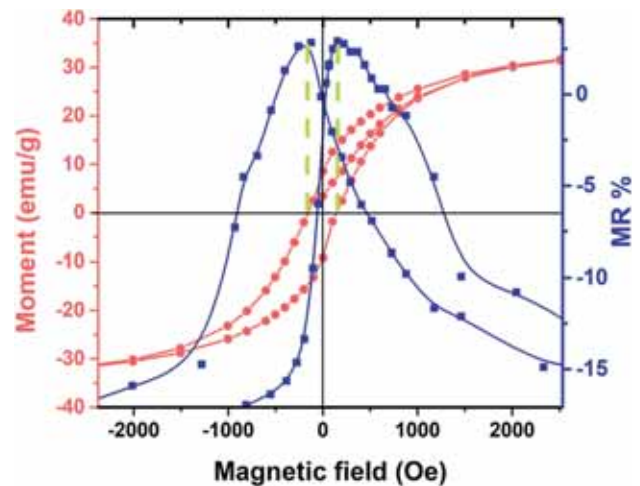


Figure 8. Low-temperature MR and $M-H$ loop of C-Ni/NiO nanocompact.

The magnetically ordered state reduces the resistance of the medium by increasing the tunnelling probability of the charge carrier through the medium. This spin-dependent tunnelling is particularly strong at low temperatures and results in large MR (-20.4%) at 18 K when compared with the observed room-temperature MR response (-4.2%) in our sample. This happens due to decrease in spin polarization magnitude (P) at 300 K, compared with 18 K. The reduction in P has been attributed to spin-disordered regions at the grain boundaries in magnetic granular systems [47,48]. Also, as the temperature is raised, the spin fluctuations increase and the scattering at spin-disordered grain boundary regions reduces the spin-polarized current.

The low-temperature MR measurement shows two distinct peaks corresponding to the maximum resistance of the sample for the applied field of nearly 160 Oe both in positive and negative sides as shown in figure 8. The magnetic field for maximum MR is almost equal to the coercive field of the sample. At the coercive field, the magnetic moments become zero, which represents the maximum-spin-disordered state of the sample [11]. The maximum disorder in moments is responsible for the highest electrical resistance for the applied field near coercive field due to large electron–spin scattering. The observed sharp low-field MR response can also be attributed to spin-dependent tunnelling of spin-polarized conduction electrons through grain or domain boundaries in polycrystalline nanocompact [49]. Additionally, the peak in MR curve at coercive field could arise due to the field-induced alignment of magnetization of contiguous grains [13]. The graphitic carbon coating, along with insulating NiO layer, acts as inter-bridging and tunnelling barrier between the adjacent FM Ni cores, which leads to efficient spin-dependent tunnelling even at room temperature. The overall MR has dominant contribution from spin-dependent tunneling, besides other mechanisms.

4. Conclusions

The carbon-coated Ni/NiO nanocomposite was successfully synthesized by a chemical route. Structural studies revealed the presence of graphite, Ni and NiO in the nanocomposite with NiO as the majority phase. It shows an SPM behaviour at room temperature with $T_B \sim 290$ K. The nanocomposite exhibits exchange bias effect with loop shift in $M-H$ loop by ~ 76 Oe at 10 K in 1 T cooling field. Large negative MR of $\sim 4\%$ was observed at room temperature for applied field of 5 kOe, which increased to $\sim 20\%$ at 18 K. The large value of MR is ascribed to the electron–spin scattering and spin-dependent tunnelling of current through the well-connected NPs in the nanocomposite along with reduced spin fluctuations and lower defect density at low temperature.

Acknowledgements

Authors thank Prof G U Kulkarni for the constant support and encouragement. SA thanks SERB for funding under EMR (EMR/2016/005081). SR and RK thank CeNS for JRF and post-doctoral fellowships, respectively.

References

- [1] Prinz G A 1998 *Science* **282** 1660
- [2] Wolf S A, Awschalom D D, Buhrman R A, Daughton J M, von Molnár S, Roukes M L *et al* 2001 *Science* **294** 1488
- [3] Reig C, Cubells-Beltrán M D and Ramírez Muñoz D 2009 *Sensors* **9** 7919
- [4] Daughton J M 1997 *J. Appl. Phys.* **81** 3758
- [5] Wang W, Wang Y, Tu L, Feng Y, Klein T and Wang J P 2014 *Sci. Rep.* **4** 5716
- [6] Baibich M N, Broto J M, Fert A, Van Dau F N, Petroff F, Etienne P *et al* 1988 *Phys. Rev. Lett.* **61** 2472
- [7] Yang F Y, Liu K, Hong K, Reich D H, Searson P C and Chien C L 1999 *Science* **284** 1335
- [8] Matveev K A, Glazman L I, Clarke P, Ephron D and Beasley M R 1995 *Phys. Rev. B* **52** 5289
- [9] Xing H, Kong W, Kim C, Peng S, Sun S, Xu Z A *et al* 2009 *J. Appl. Phys.* **105** 063920
- [10] Parkin S S P 1995 *Annu. Rev. Mater. Sci.* **25** 357
- [11] Xiao J Q, Jiang J S and Chien C L 1992 *Phys. Rev. Lett.* **68** 3749
- [12] Liu K, Zhao L, Klavins P, Osterloh F E and Hiramatsu H 2003 *J. Appl. Phys.* **93** 7951
- [13] Coey J M D, Berkowitz A E, Balcells L, Putris F F and Parker F T 1998 *Appl. Phys. Lett.* **72** 734
- [14] Chien C L, Xiao J Q and Jiang J S 1993 *J. Appl. Phys.* **73** 5309
- [15] Zeng H, Black C T, Sandstrom R L, Rice P M, Murray C B and Sun S 2006 *Phys. Rev. B* **73** 020402
- [16] Yuasa S and Djayaprawira D D 2007 *J. Phys. D: Appl. Phys.* **40** R337
- [17] Williams G V M, Prakash T, Kennedy J, Chong S V and Rubanov S 2018 *J. Magn. Magn. Mater.* **460** 229
- [18] Allia P, Coisson M, Tiberto P, Vinai F, Knobel M, Novak M A *et al* 2001 *Phys. Rev. B* **64** 144420
- [19] Jones F W 1938 *Proc. R. Soc. Lond.* **166** 16
- [20] Mironova-Ulmane N, Kuzmin A, Steins I, Grabis J, Sildos I and Pārs M 2007 *J. Phys. Conf. Ser.* **93** 012039
- [21] Pimenta M A, Dresselhaus G, Dresselhaus M S, Cancado L G, Jorio A and Saito R 2007 *Phys. Chem. Chem. Phys.* **9** 1276
- [22] Patange M, Biswas S, Yadav A K, Jha S N and Bhattacharyya D 2015 *Phys. Chem. Chem. Phys.* **17** 32398
- [23] Akbarzadeh A, Samiei M and Davaran S 2012 *Nanoscale Res. Lett.* **7** 144
- [24] Chen Q and Zhang Z J 1998 *Appl. Phys. Lett.* **73** 3156
- [25] Fonseca F C, Goya G F, Jardim R F, Muccillo R, Carreño N L V, Longo E *et al* 2002 *Phys. Rev. B* **66** 104406
- [26] Ramírez-Meneses E, Betancourt I, Morales F, Montiel-Palma V, Villanueva-Alvarado C C and Hernández-Rojas M E 2011 *J. Nanopart. Res.* **13** 365
- [27] Singh J, Patel T, Kaurav N and Okram G S 2016 *AIP Conf. Proc.* **1731** 050036
- [28] Duan W J, Lu S H, Wu Z L and Wang Y S 2012 *J. Phys. Chem. C* **116** 26043
- [29] Shim H, Manivannan A, Seehra M S, Reddy K M and Punnoose A 2006 *J. Appl. Phys.* **99** 08Q503
- [30] Roy A, De Toro J A, Amaral V S, Muniz P, Riveiro J M and Ferreira J M F 2014 *J. Appl. Phys.* **115** 073904
- [31] Peddis D, Rinaldi D, Ennas G, Scano A, Agostinelli E and Fiorani D 2012 *Phys. Chem. Chem. Phys.* **14** 316201
- [32] Roy S, Kambhala N and Angappane S 2018 *AIP Conf. Proc.* **1942** 050082
- [33] Parada C and Morán E 2006 *Chem. Mater.* **18** 2719
- [34] Del Bianco L, Spizzo F, Tamisari M and Castiglioni A 2011 *J. Appl. Phys.* **110** 043922
- [35] Ganeshchandra Prabhu V, Shajira P S, Lakshmi N and Junaidd Bushiri M 2015 *J. Phys. Chem. Solids* **87** 238
- [36] Li Z, Su Y, Liu Y, Wang J, Geng H, Sharma P *et al* 2014 *CrystEngComm* **16** 8442
- [37] Kodama R H, Berkowitz A E, McNiff J E J and Foner S 1996 *Phys. Rev. Lett.* **77** 394
- [38] Berkowitz A E and Takano K 1999 *J. Magn. Magn. Mater.* **200** 552
- [39] Meiklejohn W H 1962 *J. Appl. Phys.* **33** 1328
- [40] Del Bianco L, Boscherini F, Fiorini A L, Tamisari M, Spizzo F, Antisari M V *et al* 2008 *Phys. Rev. B* **77** 094408
- [41] Sharma S K, Vargas J M, Knobel M, Pirota K R, Meneses C T, Kumar S *et al* 2010 *J. Appl. Phys.* **107** 09D725
- [42] Feyngenson M, Kou A, Kreno L E, Tiano A L, Patete J M, Zhang F *et al* 2010 *Phys. Rev. B* **81** 014420
- [43] Parkin S S P, Li Z G and Smith D 1991 *J. Appl. Phys. Lett.* **58** 2710
- [44] Chappert C, Fert A and Van Dau F N 2007 *Nat. Mater.* **6** 813
- [45] Fullerton E E, Kelly D M, Guimpel J, Schuller I K and Bruynseraede Y 1992 *Phys. Rev. Lett.* **68** 859
- [46] Pol S V, Pol V G, Frydman A, Churilov G N and Gedanken A 2005 *J. Phys. Chem. B* **109** 9495
- [47] Serrate D, De Teresa J M, Algarabel P A, Ibarra M R and Galibert J 2005 *Phys. Rev. B* **71** 104409
- [48] Prakash T, Williams G V M, Kennedy J and Rubanov S 2016 *J. Appl. Phys.* **120** 123905
- [49] Hwang H Y, Cheong S W, Ong N P and Batlogg B 1996 *Phys. Rev. Lett.* **77** 2041